Letter | Editors' Suggestion

Tuning heat transport in graphene by tension

H. Liu [1,*] M. Lee,[2] M. Šiškins,[1,2] H. S. J. van der Zant,[2] P. G. Steeneken [1,2] and G. J. Verbiest [1,†]

[1]*Department of Precision and Microsystems Engineering, Delft University of Technology, Mekelweg 2, 2628 CD Delft, The Netherlands*

[2]*Kavli Institute of Nanoscience, Delft University of Technology, Lorentzweg 1, 2628 CJ Delft, The Netherlands*

(Received 17 November 2022; revised 17 July 2023; accepted 19 July 2023; published 2 August 2023)

Heat transport by acoustic phonons in two-dimensional (2D) materials is fundamentally different from that in 3D crystals because the out-of-plane phonons propagate in a unique way that strongly depends on tension and bending rigidity. Here, using optomechanical techniques, we experimentally demonstrate that the heat transport time in freestanding graphene membranes is significantly higher than the theoretical prediction, and decreases by as much as 33% due to an electrostatically induced tension of 0.07 N/m. Using phonon scattering and Debye models, we explain these observations by the tension-enhanced acoustic impedance match of flexural phonons at the boundary of the graphene membrane. Thus, we experimentally elucidate the tunability of phononic heat transport in 2D materials by tension, and open a route towards electronic devices and circuits for high-speed control of temperature at the nanoscale.

DOI: 10.1103/PhysRevB.108.L081401

Although in most bulk materials the propagation speed of different types of acoustic phonons is of similar magnitude, the situation is vastly different in two-dimensional (2D) materials [1–5]. In these atomically thin materials, in-plane phonons have a constant propagation speed that is determined by the atomic bond stiffnesses, whereas out-of-plane flexural phonons exhibit a frequency-dependent speed that is determined by both in-plane strain and bending rigidity [6–9], such that flexural and in-plane phonon velocities can differ by more than an order of magnitude. Initial studies suggested that flexural phonons provide the dominant pathway for heat transport and storage in 2D materials [10,11], however, it has been difficult to experimentally separate flexural and in-plane phonon contributions.

Evidence for the importance of speed differences on the phononic heat transport in 2D materials was provided by a theoretical analysis [12] and by the experimental observation of two distinct thermal time constants in graphene membranes, of which the longest, τ, is a probe for studying heat transport by the relatively slow flexural phonons [13–17]. To understand heat propagation via these different in-plane and out-of-plane phononic channels in 2D materials, studies of the role of flexural phonons are essential. Yet, unlike the lattice thermal conductivity of 2D materials, which has been well characterized by Raman microscopy [18,19], a microscopic picture of how the rate of heat transport is related to the properties of flexural phonons remains elusive, as it requires a methodology for measuring their effect on temperature variations in suspended 2D materials with nanosecond resolution.

In this Letter, we demonstrate that heat flow in graphene can be tuned by tension using an optothermomechanical method to experimentally characterize heat transport in graphene drum resonators with nanosecond resolution. We control the tension by an electrostatic force induced by a voltage V_g on a gate underneath the graphene drum. Using an optothermal drive, we actuate the graphene drum resonators [20]. From the mechanical resonance frequency $\omega_0/(2\pi)$ (>10 MHz) as a function of V_g, we determine the in-plane tension and effective mass of the drum, and from the mechanical response at low frequencies (<1 MHz), we extract the thermal time constant τ of the resonators that describes the time for heat propagating from the center to the boundary of the membrane. To explain the observed tension dependence of τ, we combine the Debye model for phononic heat transport with a boundary scattering model that describes acoustic phonon reflection and transmission at the edge of the graphene drum. From this analysis it follows that heat transport mainly depends on tension due to its effect on the acoustic impedance match between the flexural phonons on the suspended and supported part of membrane.

Four graphene drum resonators, devices D1–D4, are measured to study the effect of tension on heat transport, as shown in Figs. 1(a) and 1(b). The surface profile measured by atomic force microscopy indicates an initial downward deflection of the membrane, resulting from sidewall adhesion at the edge of the membrane [21] [see Fig. 1(c)]. We measure the motion of the resonators using the interferometer depicted in Fig. 1(d). By exciting the membrane with a modulated blue laser, while interferometrically detecting its motion, the frequency response of the devices is determined and used to characterize both the mechanical and thermal parameters of the devices. Figure 1(e) shows the measured motion amplitude z_ω of device D1 at $V_g = 0$ V over the frequency range from 0.1 to 100 MHz. We extract $\omega_0/(2\pi)$ and quality factor Q of the device by fitting the measured data to a harmonic oscillator model [Fig. 1(f)]. For device D1 this results in $\omega_0/(2\pi) = 25.49$ MHz and $Q = 43.25$. The average quality factor of the four devices at room temperature is $Q = 36.5 \pm 8.4$, which

*H.Liu-7@tudelft.nl
†G.J.Verbiest@tudelft.nl

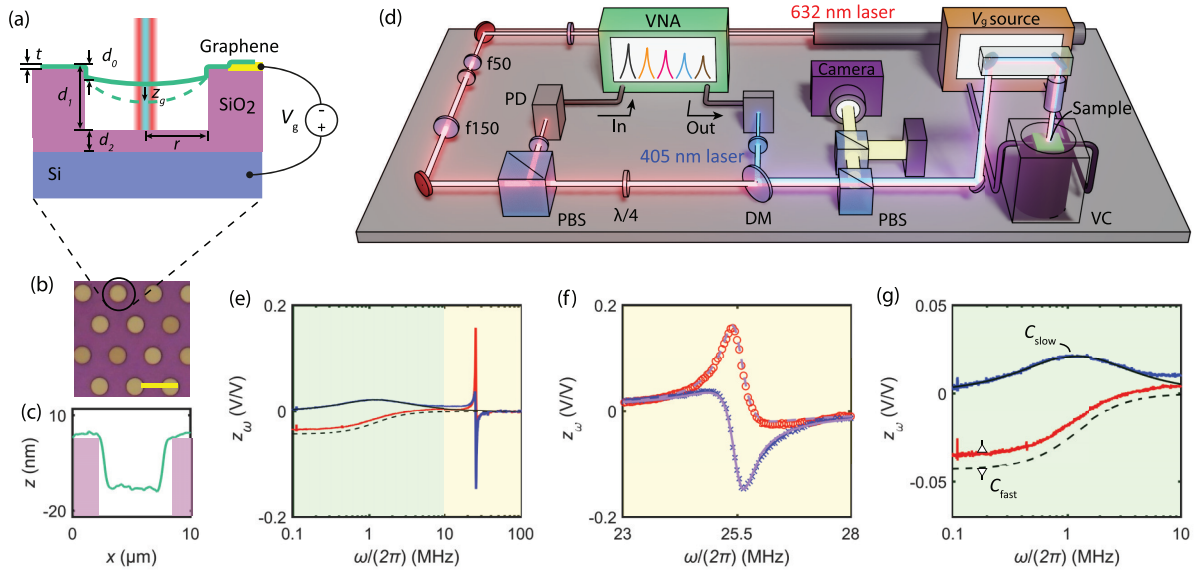

FIG. 1. Graphene membrane characterization. (a) Schematic of a graphene drum of radius r over a cavity of depth d_1 in a SiO_2/Si substrate irradiated by lasers. The graphene has a sidewall of length d_0 into the cavity. The voltage V_g pulls the drum down by z_g, increasing its tension. (b) Optical image of the drums with a scale bar of 10 μm. (c) Atomic force microscope line trace over device D4 indicates a downward deformation of drum, originating a kink at the boundary. Note the different units for x and z on the axis. (d) Interferometric setup. The sample is placed inside a vacuum chamber (VC). The blue (405 nm) laser is intensity modulated by a vector network analyzer (VNA) to actuate the resonator. Intensity variations of the reflected red (633 nm) laser caused by resonator motion, are measured by a photodiode (PD) and recorded with the VNA. PBS: polarized beam splitter; DM: dichroic mirror. (e) Frequency response of device D1, including real (red) and imaginary (blue) parts of the motion z_ω. (f) Fits of $z_\omega/(2\pi)$ (lines) to Eq. (1) to obtain ω_0. (g) Fits of Eq. (1) to z_ω near the thermal peak (black solid and dashed lines) provide τ, $C_{\rm fast}$, and $C_{\rm slow}$ of the resonator.

is comparable to literature values [22,23]. Around 1 MHz, we observe an additional broad signal in the imaginary part of the frequency response [Fig. 1(g)]. This signal is associated [20] with the frequency-dependent optothermal force $F_{{\rm th},\omega}$ on the resonator, because it is only present when driving the membrane optothermally. Following literature [13], far below mechanical resonance, the displacement $z_\omega = F_{{\rm th},\omega}/k$ is proportional to the effective thermal expansion force $F_{{\rm th},\omega}$ that is delayed with respect to the laser power $P(t) = P_{\rm ac}e^{i\omega t}$ as a consequence of the time τ it takes to increase the membrane temperature by laser heating. As shown by the fits in Fig. 1(g), the low-frequency z_ω is given by

$$z_\omega = \frac{C_{\rm slow}}{1 + i\omega\tau} + C_{\rm fast}, \tag{1}$$

where $C_{\rm slow}$ and $C_{\rm fast}$ are the normalized thermal expansion amplitudes contributed from out-of-plane and in-plane phonons, respectively [13]. We extract these parameters by fitting Eq. (1) to the real and imaginary parts of the measured z_ω, as depicted in Fig. 1(g). Here, the peak in the imaginary part of z_ω is located at 1.23 MHz, corresponding to $\tau = (2\pi \times 1.23\ {\rm MHz})^{-1} = 129$ ns. We checked the laser power dependence and verified that it has no significant effect on the measured value of τ (see Figs. S1(a) and S1(b) in [24]).

By applying $V_{\rm g}$ on graphene drum resonators, we observe a clear change in both the measured $\omega_0/(2\pi)$ and τ (see Fig. 2). $V_{\rm g}$ generates an electrostatic force, pulling the drum down and thereby increasing tension. Figure 2(a) shows plots of $\omega_0/(2\pi)$ against $V_{\rm g}$ for all devices from −4 to 4 V. The typical W-shaped curves show both electrostatic softening and tension hardening, as often observed in electrostatic gate tuning of graphene membranes [22]. The observed values of τ, of all above 75 ns, are significantly higher than the value of $\tau \approx 2$ ns obtained from the theoretical expression $\tau = r^2\rho_g c_p/(2k)$, that follows from solving the heat equation for a perfect circular graphene membrane [37] for typical values of specific heat c_p and thermal conductivity k. Interestingly, it

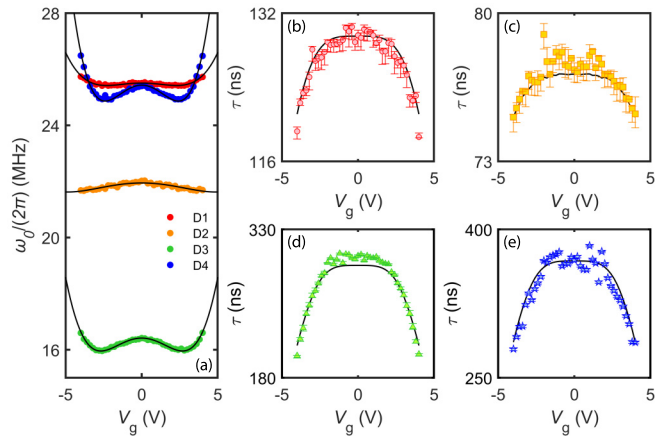

FIG. 2. Tuning thermodynamic properties of graphene drum devices with gate voltage. (a) Solid dots: ω_0 vs $V_{\rm g}$ measured in devices D1–D4; drawn lines: fits based on Eq. (2). (b)–(e) Points: τ vs $V_{\rm g}$ measured in devices D1–D4, respectively; solid lines: fits to data using the Debye and scattering models; error bars are from the fits to the measured thermal signals as plotted in Fig. 1(g).

is also shown here that τ reduces by as much as 33% when the tension in the membrane is increased by V_g [Figs. 2(b)–2(d)]. This n-dependent decrease in τ is unexpected from the heat equation, because recent studies show that c_p increases [38] while k decreases [39,40] as the tension in graphene increases, from which one would expect τ to increase at higher n, precisely opposite to our experimental observations.

To shed light on the obtained large magnitude of τ and its negative dependence on V_g-induced tension in Figs. 2(b)–2(e), we first quantify n in the drum. Following literature [22], we model $\omega_0/(2\pi)$ tuning of the drum resonator by continuum mechanics,

$$\omega_0(V_g) = \sqrt{\frac{1}{m_{\text{eff}}}\left[\frac{2\pi E t s_0}{1-\upsilon^2} + \frac{8\pi E t}{(1-\upsilon^2)r^2}z_g^2 - \frac{1}{2}\frac{\partial^2 C_g}{\partial z_g^2}V_g^2\right]}, \tag{2}$$

in which s_0 is the built-in strain, m_{eff} is the modal mass of the fundamental mode of the circular membrane resonator with a theoretical value $m_{\text{eff,th}} = 0.271\pi r^2\rho_g$ where ρ_g is the mass density of double-layer graphene, C_g is the capacitance between membrane and bottom gate, and the second derivative $\frac{\partial^2 C_g}{\partial z_g^2}$ quantifies the electrostatic softening. The 2D Young's modulus $Et \approx 175.39$ N/m on average and the Poisson ratio $\upsilon = 0.16$ were determined via atomic force microscopy (AFM) indentation [41] [see Supplemental Material (SM) Sec. 1 [24]]. The center deflection z_g can be expressed [42] as $\varepsilon_0 r^2 V_g^2/(8g_0^2 n_0)$, where $n_0 = Es_0/(1-\upsilon)$ is the pretension, ε_0 is the permittivity of vacuum, and $g_0 = d_1 + d_2/\varepsilon_{SiO_2} - d_0$ is the effective gap between the drum and the electrostatic gate. We fit the measured V_g dependence of ω_0 by Eq. (2) [black lines in Fig. 2(a)] to extract the fit parameters n_0, m_{eff}, and $\frac{\partial^2 C_g}{\partial z^2}$ for each device (listed in Table S1 [24]). The extracted initial tension n_0 for all devices ranges from 0.18 to 0.34 N/m, which corresponds to typical literature values reported for graphene membranes [22,42–44]. We attribute the variation in shapes of $\omega_0/(2\pi)$ vs V_g among devices D1–D4 to the different n_0 and m_{eff} of the membranes [22]. The good quality of the fits with Eq. (2) in Fig. 2(a) (drawn lines) allows us to use the obtained fit parameters to extract the membrane deflection z_g at all V_g. By using the equation [22] $n = n_0(1 + 4z_g^2/r^2)$, we obtain the corresponding membrane tension $n(V_g)$.

Since the classical heat equation clearly does not suffice to account for the observed τ and its tension dependence, we now will use a phonon scattering model to assess the transient thermal conduction in the membrane [12]. This model assumes that the in-plane and out-of-plane phonon baths are decoupled from each other except from the scattering at the boundary. Moreover, we neglect any heat transport through polymer residues left over after fabrication as its thermal conductivity (0.2 W/mK) is much lower than that of graphene (>1000 W/mK) [18,45]. The kink at the membrane edge [Fig. 1(c)] is the main source of n-dependent phonon scattering [46] (see Fig. S2 [24]) and results in the following expression for τ,

$$\tau = \frac{r}{2c_z\sum_j \overline{w}_{1z\to 2j}}, \quad j = l, t, z, \tag{3}$$

in which the transmission rate $\overline{w}_{1z\to 2j}$ is the probability that a flexural phonon on the suspended part of the graphene (subscript 1) is transmitted across the membrane edge and becomes a phonon of type j on the supported part of the graphene (subscript 2), where j can either be a flexural phonon ($j = z$), or a longitudinal or transverse in-plane phonon ($j = l, t$). $\overline{w}_{1z\to 2j}$ depends both on n and on the speed of sound c_z of flexural phonons (see SM Sec. 2 [24]). Due to the scattering at the edge of the membrane, the calculated magnitude of $\overline{w}_{1z\to 2j}$ is much lower than 1, which results in a value of τ that is much larger than the value $\tau = r^2\rho_g c_p/(2k)$ in the absence of scattering. This scattering is a kind of Kapitza thermal boundary resistance [47] and thus potentially accounts for the large value of τ observed in our fabricated graphene resonators [Figs. 2(b)–2(e)]. We also calculated the contribution of in-plane phonons to τ using the scattering model and found that it is much smaller than the contribution of flexural phonons (see SM Sec. 2 [24]). Therefore, we only consider the incidence of flexural phonons in Eq. (3).

Heat is transported by phonons of many different frequencies, while $\overline{w}_{1z\to 2j}$ depends on the speed of these phonons. Therefore, to analyze the effect of tension on heat transport, the dispersion relation for flexural phonons is needed, which is given [48] by $\omega_q = \sqrt{(\kappa q^4 + nq^2)/(\eta\rho_g)}$, where q is the wave number, κ is the bending rigidity of the membrane, and $\eta = m_{\text{eff}}/(0.271\pi r^2\rho_g)$ is the normalized areal density of the membrane (listed in Table S1 for all devices [24]). This dispersion relation is in line with the results of studies from first principles (from the Γ to K point) [49], from which the speed of sound for flexural phonons is found using $c_z = \frac{\partial\omega_q}{\partial q}$.

We now theoretically estimate the thermal time constant of graphene drum resonators. In practice, flexural phonons over a large frequency span, ranging up to the Debye frequency ω_{qd}, will contribute to τ. Note that the frequency of flexural phonons is much larger than that of $1/\tau$, since τ describes the timescale of thermal expansion of the entire membrane. To account for this [see the flow chart in Fig. S6(a) [24]], we analyze the heat transport contribution for every q using the tension-dependent phonon speed $c_z(\omega_q, n)$ and determine the thermal time constant for phonons of that wave number $\tau(\omega_q, n)$ using Eq. (3). Then, we use the Bose-Einstein distribution to determine the expected phonon energy density via the specific heat spectral density $C^z_{v,\omega}(\omega_q, n)$ of flexural phonons of a certain q (Debye model). The detailed expression of $C^z_{v,\omega}(\omega_q, n)$ can be found in Eq. (S2) [24]. Finally, we take a weighted integral over the contributions of all flexural phonons to determine $\tau(n)$ using $1/\tau(n) = \int_0^{\omega_{qd}} C^z_{v,\omega}(\omega_q, n)/[C^z_v(n)\tau(\omega_q, n)]d\omega_q$, where the total specific heat due to flexural phonons is determined using $C^z_v(n) = \int_0^{\omega_{qd}} C^z_{v,\omega}(\omega_q, n)d\omega_q$ [48,50]. More details about the phononic scattering and Debye models can be found in SM Secs. 3 and 4 [24].

The obtained function $\tau(n)$ is fit to the experimental data in Figs. 2(b)–2(e), obtaining good agreement between fit and experiments for all four devices, using κ as the only fit parameter. All other model parameters are determined independently from measurements. The fitted values of κ vary over a range from 0.6 to 9.4 eV, which is similar to values reported in the literature [51,52]. Although the exact

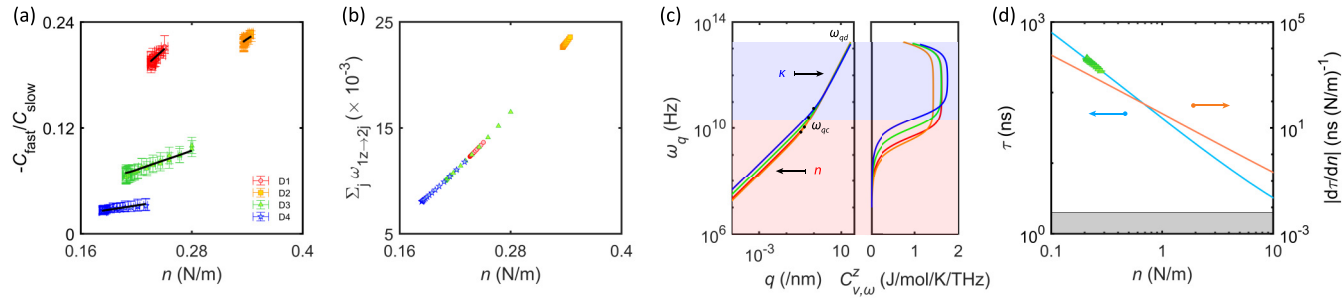

FIG. 3. Analysis and experimental demonstration on tunable heat transport in graphene drum resonators. (a) Ratio of normalized thermal expansion amplitudes $|C_{\rm fast}/C_{\rm slow}|$ vs tension n. Points: the measurements; solid lines: the modeled estimates. (b) $\sum_j \overline{w}_{1z\to 2j}$ $(j = l, t, z)$ of flexural phonons for devices D1–D4 as $c_z = 575\,{\rm m}/s$, indicating the tension-enlarged impedance matching of acoustic phonons at the boundary of membrane. This tunability is the same for all-frequency phonons with different c_z. (c) Left panel: calculated $\omega_q(q)$ for devices D1–D4. $\omega_q(q)$ is dominated by n in the ∼MHz regime (red shadow) and dominated by κ in the ∼THz regime (blue shadow), respectively, while the crossover frequency ω_{qc} is located at the ∼GHz regime. Right panel: $C^z_{v,\omega}$ for all devices. (d) Tunable τ with n varying from 0.1 to 10 N/m, using device D3 as an example. Green points: the measured τ vs n for device D3; blue line: estimated τ by the scattering model; red line: tension tunability $|d\tau/dn|$; gray region: the estimation of τ using $r^2\rho_g c_p/(2k)$.

mechanism behind these bending rigidity variations remains unclear, we observe in Fig. S6(b) that κ increases with η of the membranes [24], potentially indicating that polymer residues do not only affect the mass of the membrane, but also play an important role in the heat transport by increasing the membrane's bending rigidity.

To analyze the main mechanism by which n can reduce τ in graphene resonator, we investigate three different ways: via $c_z(n, \omega_q)$, via $C^z_{v,\omega}(n, \omega_q)$, and via $\overline{w}_{1z\to 2z}$. Since n mainly affects the dispersion relation of low-frequency (MHz) phonons, the direct impact of n on τ via the first two paths is relatively small [see Figs. S7(f) and S7(i) in SM [24]]. Therefore, the observed decrease of τ in Figs. 2(b)–2(e) is mainly attributed to the n-induced increase in $\sum_j \overline{w}_{1z\to 2j}$, as plotted in Fig. 3(b). Specifically, we see the wave amplitudes $|u_{2j}|$ of all three transmitted modes increase with n [Fig. S2(b)], indicating an enhanced impedance matching of acoustic phonons between the suspended and supported part of the membrane.

Besides τ, the normalized thermal expansion amplitudes $C_{\rm fast}$ and $C_{\rm slow}$ in Eq. (1) can provide us with more information on the heat flow. We attribute the opposite signs of $C_{\rm fast}$ and $C_{\rm slow}$ in the measurements to the opposite signs of the Grüneisen parameters for the in-plane and out-of-plane phonon modes. Here, we will use them to analyze the relative contributions of the in-plane and flexural phonons to the thermal expansion force [13], and also show that the tension dependence of these amplitudes $C_{\rm fast}$ and $C_{\rm slow}$ agrees well to the presented model. From the low-frequency fits of z_ω [see Fig. 1(g)], we determine the tension dependence of $C_{\rm fast}$ and $C_{\rm slow}$ in Eq. (1). Because the thermal expansion amplitude is proportional to the temperature increase, the measured ratio $|C_{\rm fast}/C_{\rm slow}|$ is approximately proportional to the relative temperature increase of both phonon baths [13]. Qualitatively, the n-enhanced c_z will reduce the edge scattering rate according to Eq. (3), and therefore increases the cooling rate of the flexural phonon bath. As a consequence, the temperature increase of that phonon bath and $C_{\rm slow}$ decrease [7], which leads to an increase of the ratio $|C_{\rm fast}/C_{\rm slow}|$ with n as observed in Fig. 3(a). Also shown in Fig. 3(a) (lines), our model also accurately captures the relation between n and $|C_{\rm fast}/C_{\rm slow}|$ for all devices (see more details in SM Sec. 5 [24]).

We now turn to Fig. 3(c) to get more insight in the tension tuning mechanism of τ. For high-frequency (∼THz) flexural phonons [blue shadow, Fig. 3(c)], κ dominates $\omega_q(q)$ for all devices D1–D4 [Fig. 3(c), left panel], and thus $C^z_{v,\omega}(\omega_q)$ also shows significant device-to-device variations [Fig. 3(c), right panel] which is responsible for the measured variations in τ. More details about how κ and η affect $\omega_q(q)$ and $C^z_{v,\omega}(\omega_q)$ can be found in SM Sec. 4 [24]. On the other hand, for low-frequency (∼MHz) flexural phonons [red shadow, Fig. 3(c)], the situation is completely different. The resonance frequency of the graphene membranes can be understood as a standing wave of flexural acoustic phonons and is thus proportional to the ratio $c_z \propto \sqrt{n/\eta}$ and the membrane radius, such that κ does not play an important role. c_z is thus fully determined by n and η, in line with experimental graphene resonators reported in the literature [22]. We estimate the crossover frequency ω_{qc} where the phonon dispersion $\omega_q(q)$ makes the transition from the tension n-dominated to κ-dominated regime, at around 13.5, 8.4, 27.7, and 67.3 GHz for devices D1–D4, respectively [see Fig. 3(c)].

The measured parameters (listed in Table S1 [24]) allow us to model the phonon dispersion and specific heat spectral density in Fig. 3(c) over the wide frequency range from the MHz to the THz regime. Let us discuss how this results in the tunability of the heat transport using Fig. 3(d). As n increases from 0.1 to 10 N/m, τ decreases from ∼1 μs to less than 4 ns (blue line), while the tunability $|d\tau/dn|$ also decreases significantly (orange line). In such a wide tuning of n, the tunability of heat transport is attributed not only to the increase of the transmission rate $\overline{w}_{1z\to 2j}$ of flexural phonons, but also to the increased speed of sound [$c_z \approx \sqrt{n/(\eta\rho_g)}$ for $n \gg \kappa q^2$] and the change of $C^z_{v,\omega}(n, \omega_q)$. The low τ (∼2 ns at $n = 10$ N/m) under high tension is comparable to its value obtained from the heat equation $r^2\rho_g c_p/(2k)$, demonstrating that at high tension, the heat flow rate from the center to the boundary of the membrane [20,23] [gray region, Fig. 3(d)] sets a lower limit on the acoustic phonon transport rate, whereas at low

tension the boundary scattering determines the upper limit. Understanding these limits on the tension tunability of heat transport is important for proposed applications in the field of 2D phononics, such as switchable thermal transistors, ultrasensitive thermal logic gates, and reconfigurable phononic memories [53,54].

To conclude, we measured the thermal time constant that governs nanosecond-scale heat transport in suspended graphene drums and presented experimental evidence for its tunability via gate-controlled in-plane tension. Using a Debye model that captures the scattering of acoustic phonons at the membrane edge, we present a microscopic picture of heat transport in suspended graphene membranes, where bending rigidity and tension dominate the flexural dispersion relation for THz and MHz frequency phonons, respectively. Tension is responsible for tuning the transmission rate of flexural phonons from the suspended to the supported part of the graphene. The gained insight not only advances our fundamental understanding of acoustic phonons in 2D materials, but also enables pathways for controlled and optimized thermal management in 2D-based phononic, thermoelectric, electronic, and quantum devices, as well as in 2D sensing applications such as a nanoelectromechanical system (NEMS).

P.G.S. and G.J.V. acknowledge support by the Dutch 4TU federation for the Plantenna project. H.L. acknowledges the financial support from China Scholarship Council. M.L., M.Š., H.S.J.v.d.Z., and P.G.S. acknowledge funding from the European Union's Horizon 2020 research and innovation program under Grant Agreement No. 881603 (Graphene Flagship). We thank Applied Nanolayers (ANL) for providing and transferring CVD graphene on the chips.

[1] S. Chen, Q. Wu, C. Mishra, J. Kang, H. Zhang, K. Cho, W. Cai, A. A. Balandin, and R. S. Ruoff, Thermal conductivity of isotopically modified graphene, Nat. Mater. **11**, 203 (2012).

[2] R. Wang, H. Zobeiri, Y. Xie, X. Wang, X. Zhang, and Y. Yue, Distinguishing optical and acoustic phonon temperatures and their energy coupling factor under photon excitation in nm 2D materials, Adv. Sci. **7**, 2000097 (2020).

[3] S. Lee, D. Broido, K. Esfarjani, and G. Chen, Hydrodynamic phonon transport in suspended graphene, Nat. Commun. **6**, 6290 (2015).

[4] A. Taheri, S. Pisana, and C. V. Singh, Importance of quadratic dispersion in acoustic flexural phonons for thermal transport of two-dimensional materials, Phys. Rev. B **103**, 235426 (2021).

[5] A. Cepellotti, G. Fugallo, L. Paulatto, M. Lazzeri, F. Mauri, and N. Marzari, Phonon hydrodynamics in two-dimensional materials, Nat. Commun. **6**, 6400 (2015).

[6] E. Mariani and F. von Oppen, Flexural Phonons in Free-Standing Graphene, Phys. Rev. Lett. **100**, 076801 (2008).

[7] E. V. Castro, H. Ochoa, M. I. Katsnelson, R. V. Gorbachev, D. C. Elias, K. S. Novoselov, A. K. Geim, and F. Guinea, Limits on Charge Carrier Mobility in Suspended Graphene due to Flexural Phonons, Phys. Rev. Lett. **105**, 266601 (2010).

[8] N. Bonini, J. Garg, and N. Marzari, Acoustic phonon lifetimes and thermal transport in free-standing and strained graphene, Nano Lett. **12**, 2673 (2012).

[9] H. Tornatzky, R. Gillen, H. Uchiyama, and J. Maultzsch, Phonon dispersion in MoS_2, Phys. Rev. B **99**, 144309 (2019).

[10] L. Lindsay, D. A. Broido, and N. Mingo, Flexural phonons and thermal transport in graphene, Phys. Rev. B **82**, 115427 (2010).

[11] S. Sullivan, A. Vallabhaneni, I. Kholmanov, X. Ruan, J. Murthy, and L. Shi, Optical generation and detection of local nonequilibrium phonons in suspended graphene, Nano Lett. **17**, 2049 (2017).

[12] A. K. Vallabhaneni, D. Singh, H. Bao, J. Murthy, and X. Ruan, Reliability of raman measurements of thermal conductivity of single-layer graphene due to selective electron-phonon coupling: A first-principles study, Phys. Rev. B **93**, 125432 (2016).

[13] R. J. Dolleman, G. J. Verbiest, Y. M. Blanter, H. S. J. van der Zant, and P. G. Steeneken, Nonequilibrium thermodynamics of acoustic phonons in suspended graphene, Phys. Rev. Res. **2**, 012058(R) (2020).

[14] R. J. Dolleman, D. Lloyd, M. Lee, J. S. Bunch, H. S. J. van der Zant, and P. G. Steeneken, Transient thermal characterization of suspended monolayer MoS_2, Phys. Rev. Mater. **2**, 114008 (2018).

[15] C. Metzger, I. Favero, A. Ortlieb, and K. Karrai, Optical self cooling of a deformable Fabry-Perot cavity in the classical limit, Phys. Rev. B **78**, 035309 (2008).

[16] A. Blaikie, D. Miller, and B. J. Alemán, A fast and sensitive room-temperature graphene nanomechanical bolometer, Nat. Commun. **10**, 4726 (2019).

[17] N. Morell, S. Tepsic, A. Reserbat-Plantey, A. Cepellotti, M. Manca, I. Epstein, A. Isacsson, X. Marie, F. Mauri, and A. Bachtold, Optomechanical measurement of thermal transport in two-dimensional $MoSe_2$ lattices, Nano Lett. **19**, 3143 (2019).

[18] D. Ghosh, I. Calizo, D. Teweldebrhan, E. P. Pokatilov, D. L. Nika, A. A. Balandin, W. Bao, F. Miao, and C. N. Lau, Extremely high thermal conductivity of graphene: Prospects for thermal management applications in nanoelectronic circuits, Appl. Phys. Lett. **92**, 151911 (2008).

[19] A. A. Balandin, S. Ghosh, W. Bao, I. Calizo, D. Teweldebrhan, F. Miao, and C. N. Lau, Superior thermal conductivity of single-layer graphene, Nano Lett. **8**, 902 (2008).

[20] R. J. Dolleman, S. Houri, D. Davidovikj, S. J. Cartamil-Bueno, Y. M. Blanter, H. S. J. van der Zant, and P. G. Steeneken, Optomechanics for thermal characterization of suspended graphene, Phys. Rev. B **96**, 165421 (2017).

[21] J. S. Bunch, S. S. Verbridge, J. S. Alden, A. M. van der Zande, J. M. Parpia, H. G. Craighead, and P. L. McEuen, Impermeable atomic membranes from graphene sheets, Nano Lett. **8**, 2458 (2008).

[22] C. Chen, S. Rosenblatt, K. I. Bolotin, W. Kalb, P. Kim, I. Kymissis, H. L. Stormer, T. F. Heinz, and J. Hone, Performance of monolayer graphene nanomechanical resonators with electrical readout, Nat. Nanotechnol. **4**, 861 (2009).

[23] R. J. Dolleman, D. Davidovikj, H. S. J. van der Zant, and P. G. Steeneken, Amplitude calibration of 2D mechanical resonators by nonlinear optical transduction, Appl. Phys. Lett. **111**, 253104 (2017).

[24] See Supplemental Material at http://link.aps.org/supplemental/10.1103/PhysRevB.108.L081401 for laser power-dependent measurements; details of fabrication, device parameters, acoustic phonon scattering model, and Debye model; analysis of tunable thermal time constant; and thermal nonequilibrium of acoustic phonons, which includes Refs. [25–36].

[25] G. Lopez-Polin, C. Gomez-Navarro, V. Parente, F. Guinea, M. I. Katsnelson, F. Perez-Murano, and J. Gomez-Herrero, Increasing the elastic modulus of graphene by controlled defect creation, Nat. Phys. **11**, 26 (2015).

[26] L. Lindsay, D. A. Broido, and N. Mingo, Flexural phonons and thermal transport in multilayer graphene and graphite, Phys. Rev. B **83**, 235428 (2011).

[27] D. L. Nika and A. A. Balandin, Phonons and thermal transport in graphene and graphene-based materials, Rep. Prog. Phys. **80**, 036502 (2017).

[28] H. Zobeiri, N. Hunter, R. Wang, T. Wang, and X. Wang, Direct characterization of thermal nonequilibrium between optical and acoustic phonons in graphene paper under photon excitation, Adv. Sci. **8**, 2004712 (2021).

[29] X. Cong, Q.-Q. Li, X. Zhang, M.-L. Lin, J.-B. Wu, X.-L. Liu, P. Venezuela, and P.-H. Tan, Probing the acoustic phonon dispersion and sound velocity of graphene by Raman spectroscopy, Carbon **149**, 19 (2019).

[30] T. Gunst, K. Kaasbjerg, and M. Brandbyge, Flexural-Phonon Scattering Induced by Electrostatic Gating in Graphene, Phys. Rev. Lett. **118**, 046601 (2017).

[31] N. Yang, C. Li, and Y. Tang, Effects of chirality and stacking on the thermal expansion effects of graphene, Mater. Res. Express **7**, 115001 (2020).

[32] N. Lindahl, D. Midtvedt, J. Svensson, O. A. Nerushev, N. Lindvall, A. Isacsson, and E. E. Campbell, Determination of the bending rigidity of graphene via electrostatic actuation of buckled membranes, Nano Lett. **12**, 3526 (2012).

[33] G. Wang, Z. Dai, J. Xiao, S. Z. Feng, C. Weng, L. Liu, Z. Xu, R. Huang, and Z. Zhang, Bending of Multilayer van der Waals Materials, Phys. Rev. Lett. **123**, 116101 (2019).

[34] E. Mercado, J. Anaya, and M. Kuball, Impact of polymer residue level on the in-plane thermal conductivity of suspended large-area graphene sheets, ACS Appl. Mater. Interfaces **13**, 17910 (2021).

[35] M. T. Pettes, I. Jo, Z. Yao, and L. Shi, Influence of polymeric residue on the thermal conductivity of suspended bilayer graphene, Nano Lett. **11**, 1195 (2011).

[36] L. Lindsay, W. Li, J. Carrete, N. Mingo, D. A. Broido, and T. L. Reinecke, Phonon thermal transport in strained and unstrained graphene from first principles, Phys. Rev. B **89**, 155426 (2014).

[37] R. A. Barton, I. R. Storch, V. P. Adiga, R. Sakakibara, B. R. Cipriany, B. Ilic, S. P. Wang, P. Ong, P. L. McEuen, J. M. Parpia *et al.*, Photothermal self-oscillation and laser cooling of graphene optomechanical systems, Nano Lett. **12**, 4681 (2012).

[38] K. Tada, T. Funatani, S. Konabe, K. Sasaoka, M. Ogawa, S. Souma, and T. Yamamoto, Modulations of thermal properties of graphene by strain-induced phonon engineering, Jpn. J. Appl. Phys. **56**, 025102 (2017).

[39] M. Guo, Y. Qian, H. Qi, K. Bi, and Y. Chen, Experimental measurements on the thermal conductivity of strained monolayer graphene, Carbon **157**, 185 (2020).

[40] Q. Liu and B. Xu, Anomalous thermal transport of mechanically bent graphene: Implications for thermal management in flexible electronics, ACS Appl. Nano Mater. **5**, 13180 (2022).

[41] M. Šiškins, M. Lee, D. Wehenkel, R. van Rijn, T. W. de Jong, J. R. Renshof, B. C. Hopman, W. S. Peters, D. Davidovikj, H. S. J. van der Zant *et al.*, Sensitive capacitive pressure sensors based on graphene membrane arrays, Microsyst. Nanoeng. **6**, 102 (2020).

[42] P. Weber, J. Guttinger, I. Tsioutsios, D. E. Chang, and A. Bachtold, Coupling graphene mechanical resonators to superconducting microwave cavities, Nano Lett. **14**, 2854 (2014).

[43] M. Will, M. Hamer, M. Muller, A. Noury, P. Weber, A. Bachtold, R. V. Gorbachev, C. Stampfer, and J. Guttinger, High quality factor graphene-based two-dimensional heterostructure mechanical resonator, Nano Lett. **17**, 5950 (2017).

[44] X. Zhang, K. Makles, L. Colombier, D. Metten, H. Majjad, P. Verlot, and S. Berciaud, Dynamically-enhanced strain in atomically thin resonators, Nat. Commun. **11**, 5526 (2020).

[45] W. Cai, A. L. Moore, Y. Zhu, X. Li, S. Chen, L. Shi, and R. S. Ruoff, Thermal transport in suspended and supported monolayer graphene grown by chemical vapor deposition, Nano Lett. **10**, 1645 (2010).

[46] R. J. Dolleman, Y. M. Blanter, H. S. J. van der Zant, P. G. Steeneken, and G. J. Verbiest, Phonon scattering at kinks in suspended graphene, Phys. Rev. B **101**, 115411 (2020).

[47] R. Peterson and A. Anderson, The Kapitza thermal boundary resistance, J. Low Temp. Phys. **11**, 639 (1973).

[48] T. Nihira and T. Iwata, Temperature dependence of lattice vibrations and analysis of the specific heat of graphite, Phys. Rev. B **68**, 134305 (2003).

[49] A. I. Cocemasov, D. L. Nika, and A. A. Balandin, Engineering of the thermodynamic properties of bilayer graphene by atomic plane rotations: the role of the out-of-plane phonons, Nanoscale **7**, 12851 (2015).

[50] D. Singh, J. Y. Murthy, and T. S. Fisher, Mechanism of thermal conductivity reduction in few-layer graphene, J. Appl. Phys. **110**, 044317 (2011).

[51] E. Han, J. Yu, E. Annevelink, J. Son, D. A. Kang, K. Watanabe, T. Taniguchi, E. Ertekin, P. Y. Huang, and A. M. van der Zande, Ultrasoft slip-mediated bending in few-layer graphene, Nat. Mater. **19**, 305 (2020).

[52] Y. Wei, B. Wang, J. Wu, R. Yang, and M. L. Dunn, Bending rigidity and Gaussian bending stiffness of single-layered graphene, Nano Lett. **13**, 26 (2013).

[53] M. Maldovan, Sound and heat revolutions in phononics, Nature (London) **503**, 209 (2013).

[54] A. A. Balandin, Phononics of graphene and related materials, ACS Nano **14**, 5170 (2020).